Applied Physics Letters

Large photovoltaic response in rare-earth doped $BiFeO_3$ polycrystalline thin films near morphotropic phase boundary composition

Cite as: Appl. Phys. Lett. **114**, 173901 (2019); https://doi.org/10.1063/1.5090911
Submitted: 31 January 2019 . Accepted: 14 April 2019 . Published Online: 29 April 2019

Pranab Parimal Biswas, Subhajit Pal, V. Subramanian, and P. Murugavel

Applied Physics Letters ARTICLE scitation.org/journal/apl

Large photovoltaic response in rare-earth doped $BiFeO_3$ polycrystalline thin films near morphotropic phase boundary composition

Cite as: Appl. Phys. Lett. **114**, 173901 (2019); doi: 10.1063/1.5090911
Submitted: 31 January 2019 · Accepted: 14 April 2019 ·
Published Online: 29 April 2019

View Online Export Citation CrossMark

Pranab Parimal Biswas, Subhajit Pal, V. Subramanian, and P. Murugavel[a)]

AFFILIATIONS

Department of Physics, Indian Institute of Technology Madras, Chennai 600036, India

[a)]Author to whom correspondence should be addressed: muruga@iitm.ac.in

ABSTRACT

The photovoltaic (PV) properties of polycrystalline $Bi_{1-x}La_xFeO_3$ ($x = 0$–0.3) films have been explored. The X-ray diffraction study reveals that there is a gradual phase transition with the increase in La doping. The composition $x = 0.25$ is found to be the morphotropic phase boundary (MPB), beyond which the system turns into the non-/antipolar orthorhombic phase. The polarization measurements reveal improved ferroelectric properties with the maximum remanent polarization observed for the $x = 0.25$ film. A systematic study on the direct and indirect bandgaps of the films has shown a decreasing trend with composition. Interestingly, the PV studies exhibit a maximum open-circuit voltage of 1.30 V for the $x = 0.25$ film which is three times larger than the value observed for pure $BiFeO_3$ (BFO) (0.47 V). The enhanced PV response in La-doped BFO correlates with the polarization and the change in direct/indirect bandgaps associated with structural instability near the MPB composition. The approach used in this work for enhancing the PV performance in ferroelectric BFO through the combined effects of polarization, bandgaps and competing structures provides a better pathway for improving the ferroelectric PV effect.

In recent times, the research on the photovoltaic (PV) effect has attracted a lot of attention due to the increase in demand for clean, sustainable, and renewable energy sources. The popular semiconductor p-n junction based PV cells, where the separation of light generated electron-hole pairs is assisted by the electric field in the space charge region, have limitations in the open-circuit voltage (V_{OC}) as restricted by their bandgap.[1] The urge among researchers to look for new PV materials has resulted in numerous solar cells other than the conventional semiconductor solar cells such as dye sensitized solar cells, quantum dye sensitized solar cells, organic solar cells, perovskite solar cells, etc. In this regard, the study of the PV effect in ferroelectric materials has gained importance due to the observed above bandgap V_{OC}.

However, though the ferroelectric PV effect has been known since the 1970s,[2–4] the PV studies have focused only on a few systems.[3,5–10] In addition, various theories have been proposed for the ferroelectric PV mechanism in bulk and thin films. Among them, the ballistic and shift current theories are widely researched for the bulk PV effect.[11–14] In thin films, however, the depolarization field model, where the net polarization plays an important role, along with the Schottky barrier effect at the interface is considered for the ferroelectric PV effect.[15–17] Despite such an anomalous PV effect, the poor performance of ferroelectric PV in device applications is associated with the large bandgap.[18] Efforts are being made to engineer the bandgap of known ferroelectric oxides by chemical substitution.[19–21]

In this context, $BiFeO_3$ (BFO) has recently induced enormous research interest because of its large polarization (~90 $\mu C/cm^{-2}$) and low bandgap (~2.7 eV) among other ferroelectric oxides.[22,23] A polarization direction dependent PV effect is reported in epitaxial BFO thin films, but with very low V_{OC} (0.3 V).[15] The large V_{OC} (~0.9 V) reported in epitaxial BFO films with a transparent electrode is attributed to the interface effect.[24] On the other hand, the A- and B-site doping in BFO with various elements such as Mn, Nd, Sm, Co, etc., is also reported to yield substantial enhancement in PV characteristics due to their improved ferroelectric characteristics.[25–27]

It is known that piezoelectric materials with the morphotropic phase boundary (MPB) composition exhibit scintillating properties under external stimuli.[28–33] The MPB composition can be achieved in BFO by A-site substitution of trivalent rare-earth metals (RE = Sm^{3+}, Gd^{3+}, Dy^{3+}, and La^{3+}), and improved electromechanical properties

along with dielectric properties are reported in such systems.[31] Interestingly, You *et al.* witnessed enhancement in the PV effect in La-substituted epitaxial BFO films, and they attribute it to the polarization instability created by the coexistence of polar and nonpolar phases.[34] However, detailed PV characterization at the MPB composition has not yet been explored. In the present work, systematic PV studies are carried out on a series of polycrystalline $Bi_{1-x}La_xFeO_3$ (BLFO) films to demonstrate the MPB effect on them. Remarkably, we have recorded a high V_{OC} of 1.30 V for the optimal doping concentration $x = 0.25$, where MPB has been reported. The observed results are investigated based on the polarization, bandgap, and structural instability, and the results are presented in this letter.

A series of BLFO ($x = 0.0$, 0.05, 0.10, 0.15, 0.20, 0.25, and 0.30) films were fabricated on (111)Pt/Ti/SiO_2/Si(100) substrates using a chemical solution deposition method. The initial BLFO solutions were prepared using 99.9% hydrated bismuth nitrate and iron acetylacetonate by dissolving in glacial acetic acid and 2-methoxyethanol, respectively, to form a 0.1 M solution. For La doping, lanthanum acetate was mixed in a bismuth nitrate and acetic acid solution after 1 h of stirring. The final solution was spin-coated on cleaned substrates at 4000 rotations per minute for 30 s followed by drying at 450 °C for 10 min in an oven after depositing each layer. The process was repeated 18 times to get final 350 nm thick films. The films were then annealed for 1 h at 550 °C in the ambient atmosphere. The crystal structure of the films was analyzed using an X-ray diffractometer (Rigaku-Smart Lab). The optical properties were investigated using a UV-Visible spectrometer (JASCO-V-570). The ferroelectric hysteresis loops of the BLFO samples were traced using a ferroelectric tester (Radiant Technology PMF0713–334). For PV measurements, semitransparent Au dots (~200 μm diameter and ~20 nm thickness) deposited by thermal evaporation were used as top electrodes. Piezo-response force microscopy (PFM) (Park system NX10) was used to record the domain patterns along with the domain switching behavior. PV measurements were carried out in both poled and unpoled states using a Keithley high resistance electrometer (6517B) and a xenon arc lamp. To pole the samples, the voltage (across the top and bottom electrodes) just above the coercive field at the maximum electric field is maintained for 10 min for the respective compositions.

To confirm the phase formation, the X-ray diffraction (XRD) patterns were recorded on BLFO thin films on (111)Pt/TiO_2/SiO_2/Si(100) substrates, and are shown in Fig. 1(a). The patterns demonstrate the crystallization of the films without any impurity phases. The XRD patterns of BFO show a rhombohedral phase with the *R3c* space group. This is evidenced from the peak splitting observed around $2\theta \approx 32°$ as shown in Fig. 1(b), and the peaks are indexed to (104) and (110). However, Fig. 1(b) reveals that the separation angle between these two peaks decreases with an increase in La doping, suggesting a structural change at intermediate compositions. Note that at $x = 0.30$, these peaks are indexed to (112) and (200) of the orthorhombic phase. The deconvoluted magnified version of the diffraction pattern in the 2θ range 31°–33° shown in Fig. S1 clearly emphasizes the evolution of the rhombohedral diffraction peaks (104) and (110) into the orthorhombic (200) and (112) peaks with La doping in BFO films. An additional peak (021) corresponding to the orthorhombic phase can also be noticed in the deconvoluted peaks fitted with Lorentzian line shape. The observed XRD patterns are in accordance with the literature reports on La-doped epitaxial BFO thin film samples where the

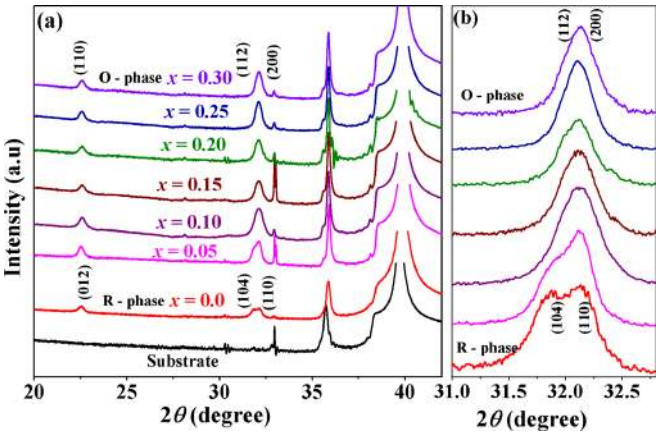

FIG. 1. (a) XRD patterns of BLFO thin films and (b) the enlarged version of the patterns in the 2θ range 31°–32.8°.

coexistence of rhombohedral and orthorhombic phases is seen at the intermediate compositions $0.10 < x < 0.30$.[31,34] Kan *et al.* have investigated detailed structural phase transitions in La-, Sm-, and Dy-substituted BFO epitaxial thin films as functions of temperature and composition. Note that they have reported similar structural transition from the rhombohedral to the orthorhombic phase for all rare-earth elements.[31] You *et al.* have also shown an analogous phase transition trend using the phase diagram drawn from the temperature variation of *P-E* hysteresis loops.[34] The reported phase diagram for BLFO thin films based on ferroelectric polarization measurements illustrates that BLFO shows a polar rhombohedral phase at $x \leq 0.10$, the coexistence of polar rhombohedral and orthorhombic phases for $0.10 < x < 0.3$, a pure antipolar orthorhombic phase for $x \approx 0.3$ and a nonpolar orthorhombic phase for $x > 0.3$.[34]

To analyze it further, the Raman spectra are recorded for BLFO thin films using the 632 nm excitation wavelength, and the respective plots are displayed in Fig. S2. The observed Raman spectra display A_1–1 and A_1–2 prominent modes which are reminiscent of the BFO rhombohedral phase for the $x = 0$ sample. These modes are found to merge into a broader peak with an increase in x favoring the observed phase transition. The XRD patterns and Raman spectra along with previous reports[31,34] suggest that the polycrystalline BLFO films show a structural change similar to the epitaxial films reported in the literature.

To understand the effect of La substitution on the bandgap of BFO thin films, UV-Vis spectroscopy measurements were performed on BLFO films. The calculated absorption coefficient α obtained from the absorption spectra is plotted in Fig. 2(a) for all samples. The prominent transitions are marked in the figure. The 1st transition marked in Fig. 2(a) originated from the charge transfer (CT) transition instability, an inherent property of iron oxides.[35] The 2nd transition marked in Fig. 2(a) corresponds to the bandgap of BFO.[36,37] Conflicting reports are seen in the literature regarding the nature of the bandgap in BFO. An indirect bandgap with $E_g = 2.0$ eV (the obtained value is subjected to the parameter chosen) is predicted by the first principles local spin-density approximation (LSDA+U) method[38,39] On the other hand, the direct bandgap is estimated for BFO by the screened exchange density functional theory

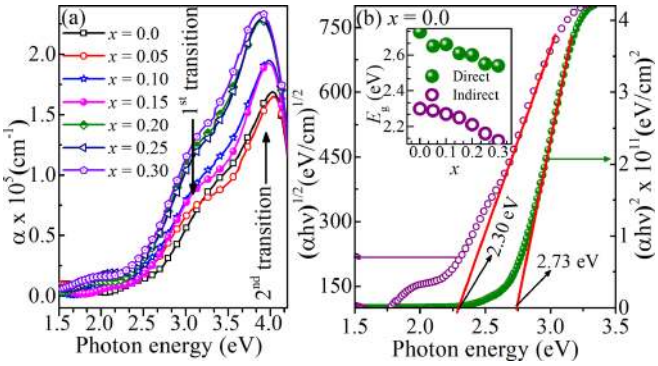

FIG. 2. (a) The α vs photon energy curve for BLFO films showing two major transitions. (b) Tauc's plots for direct and indirect bandgaps of the BFO film. The inset shows plots of calculated direct (solid symbol) and indirect (open symbol) bandgaps vs x.

approximation method.[40] To ascertain the nature of the bandgap in BLFO thin films, the direct and indirect bandgaps are calculated from Tauc's plots of $(\alpha h\nu)^n$ vs $h\nu$ as shown in Fig. 2(b) for the $x = 0.0$ film. Here, h is the Planck's constant, ν is the frequency, $n = 2$ for direct and $n = 1/2$ for indirect bandgaps.[41] The detailed discussion about two extra branches in the indirect band gap plot and the respective Tauc's plots for all other samples are given in Figs. S3 and S4, respectively. The extracted direct and indirect bandgaps are plotted as a function of x in the inset of Fig. 2(b). It is seen that La doping in BFO shifts both direct and indirect bandgaps toward lower energies (red shift). However, the reduction seen in the indirect bandgap is more pronounced compared to the change in the direct bandgap. The affinity of transition toward the indirect bandgap in La-doped BFO agrees with the theoretical prediction where it depicts bandgap evolution throughout the structural transition from rhombohedral to orthorhombic to cubic.[42] In addition, the indirect bandgap of $LaFeO_3$ also gives an indication on the direct-indirect bandgap transition.[43]

The structural evolution due to the substitution of La in the BFO system can have a prominent impact on the ferroelectric nature of the system. To probe its effect, the polarization (P) vs electric field (E) measurements are carried out on all films at room temperature, and the resultant plots are shown in Fig. 3. The figure displays that the remanent polarization (P_r) at the maximum applied field shows an increasing trend up to $x = 0.25$, where it exhibits the maximum $P_r \sim 21\ \mu C/cm^2$.

However, the P-E hysteresis loops for the film with $x = 0.30$ indicates a change in shape along with repressed remanent polarization, a trademark sign of phase evolution toward the paraelectric state. For smaller atomic radii RE dopants such as Sm^{3+}, Dy^{3+}, etc., in BFO, the P-E hysteresis loop is reported to exhibit an abrupt transformation from the single hysteresis loop (ferroelectric rhombohedral phase) to the double hysteresis loop (antiferroelectric orthorhombic phase).[36] However, with La^{3+} as the dopant, where the ionic radii of La^{3+} and Bi^{3+} are similar, the double hysteresis loop behavior becomes less prominent, and the phase transition is not abrupt.[36]

Though there are various origins given in the literature for the enhanced piezoelectric/ferroelectric response in such systems near the MPB, more accepted model is the free energy instability near a structural phase boundary.[44] This model suggests that the highest

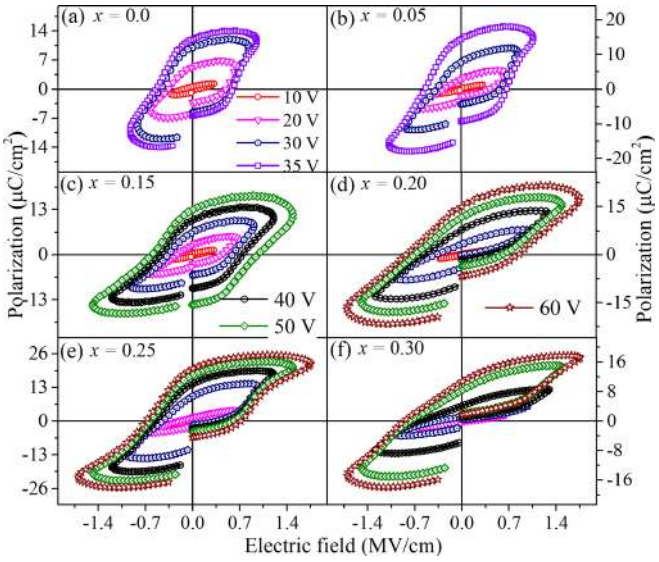

FIG. 3. (a)–(f) P-E hysteresis loops of BLFO thin films of different La concentrations.

piezoelectric/ferroelectric response is observed at the boundary between the phases where the polarization either emerges from a non-/antipolar state or changes direction across the phase boundary. The evolution of domains and the switching characteristics of all the thin film samples are recorded using the PFM measurements, and are presented in Fig. S5. The figures suggest that at $x = 0.25$, though the domains are not very prominent (signature of low piezo-response), it can be brought back to the polar state after poling. On the other hand, the $x = 0.30$ sample remains in the non-/antipolar state even after poling.

The above observed properties such as reduced bandgaps and the enhanced P-E properties near MPB due to La substitution could play a vital role in the PV response in polycrystalline BLFO films. The PV characteristics are studied in BLFO thin films in capacitor geometry, and the experimental schematic is shown in Fig. 4(a). The measurements are carried out under dark and light illumination conditions on samples with unpoled and poled states. The resultant current density (J) vs voltage (V) curves for BLFO thin films $x = 0.0$, 0.25, and 0.30 are shown in Figs. 4(b)–4(d) (the corresponding plots for other samples are displayed in Fig. S6). The samples under unpoled states reveal a typical J-V curve reminiscent of diode characteristics without any photovoltaic response. However, the samples in the poled state reveal a clear PV response with short-circuit current density (J_{SC}) and open-circuit voltage (V_{OC}).

Interestingly, the J-V curves recorded in the positive poled (Au dots and the Pt electrode are connected to positive and negative terminals, respectively) and negative poled states illustrate switchable PV characteristics. Among all samples, the film with $x = 0.25$ exhibits remarkably large V_{OC} values of -1.30 V and $+0.96$ V in +ve and −ve poled states, respectively. The switchable nature of V_{OC} upon change in poling directions indicates that the polarization (the resultant depolarization field E_{dp} due to incomplete screening of surface bound charges) plays a dominating role in the observed PV effect. However,

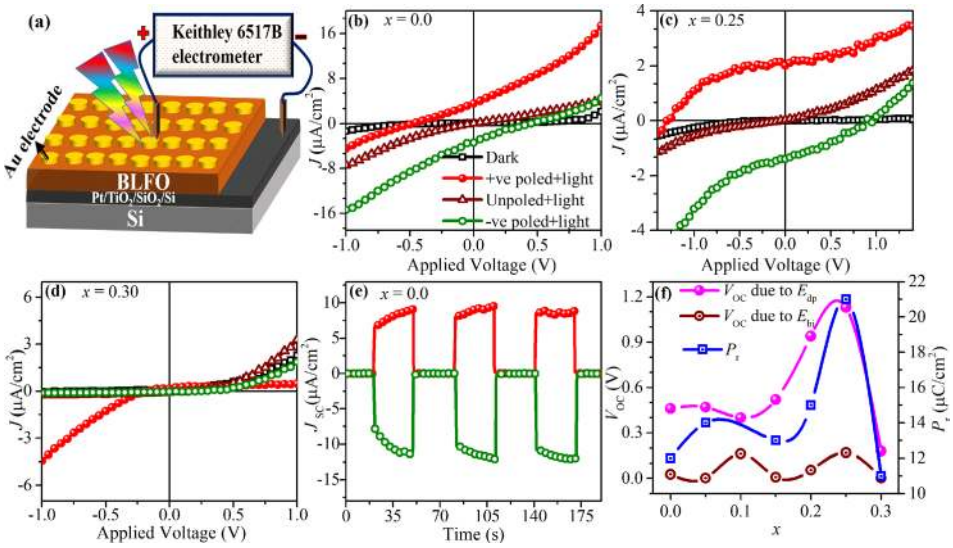

FIG. 4. (a) Schematic diagram of the PV measurement set-up, (b)–(d) the dark and light illuminated *J*-V curves of BLFO thin films for $x = 0.0$, 0.25, and 0.30 measured in unpoled and poled states, (e) current density plotted vs time in the light OFF-ON state for the BFO sample, and (f) estimated V_{OC}'s due to E_{dp} (solid sphere), E_{bi} (open circle) and remanent polarization P_r (open square) as a function of x.

the observed difference in the magnitude of V_{OC} between the poling states suggests additional contributions from the electrode/film interfaces (the resultant built-in field E_{bi}). To probe the switchable nature of the PV response further, the transient current measurements are carried out at zero-bias under light ON and OFF conditions on all films in both poled states. As a representative example, the corresponding J_{SC} vs time for the BFO film is shown in Fig. 4(e). The figure displays a sharp current response in light ON and OFF states. The difference in the magnitude of J_{SC} seen in Fig. 4(e) between positive and negative poled conditions may arise from the asymmetric electrode contributions. The repeatability of the PV characteristics is verified on pure BFO samples by measuring the *J* vs V for 5 cycles of both positive and negative poling states. The results shown in Fig. S7 indicate the stability of the PV response in the BFO sample.

The switchable and unswitchable components of V_{OC} due to E_{dp} and E_{bi} are estimated using $\frac{1}{2}(V_+ - V_-)$ and $\frac{1}{2}(V_+ + V_-)$, respectively.[15] Here, V_+ and V_- are the respective V_{OC}'s obtained in positive and negative poled states. The resultant V_{OC}'s are plotted as a function of x in Fig. 4(f). The plots reiterate the dominance of the polarization effect as compared to the interfacial effect. This is further evidenced from the remanent polarization plotted as a function of composition in Fig. 4(f) which shows a similar trend as V_{OC} with composition. Interestingly, the E_{dp} contribution of V_{OC} is found to show enhanced values between the composition $x = 0.15$–0.25 with a maximum of 1.13 V displayed by the $x = 0.25$ film. On the other hand, the E_{bi} contribution is just 0.17 V for the same composition. Notably, the contribution from E_{dp} is ~6.6 times larger than the contribution from E_{bi}. Note that La substitution in BFO creates structural instability at MPB ($x = 0.25$) which, in turn, affects the charge transfer at the band edges and drives a direct to indirect bandgap transition. The reduction in the direct bandgap increases the optical absorption; on the other hand, the reduction in the indirect bandgap minimizes the radiative recombination of thermalized photogenerated carriers, thus improving the PV effect. Though the bandgaps show a decreasing trend with further La doping ($x > 0.25$), the system turns into a paraelectric state, hence preventing it from showing any PV effect. The structural instability also enhances the polarization, thereby emphasizing the correlation between bandgaps, polarization, and MPB. Therefore, the large increment in the PV response in the compositions near MPB could be associated with the combined effects of structural instability, decrease in direct and indirect bandgaps, and improved polarization characteristics at MPB upon La substitution.

In summary, the photovoltaic studies on a series of $Bi_{1-x}La_xFeO_3$ ($x = 0.0$, 0.05, 0.1, 0.15, 0.20, 0.25, and 0.30) polycrystalline films fabricated on Pt(111)/TiO/SiO_2/Si(100) substrates revealed an enhanced PV effect for $0.10 < x < 0.30$ compositions. The structural studies unveil the coexistence of rhombohedral and orthorhombic phases in this composition range. Interestingly, the film with $x = 0.25$, which is the MPB composition (beyond which the system changes to the anti-/nonpolar orthorhombic phase), shows the maximum polarization and V_{OC}. It is noteworthy to mention that all samples show both direct and indirect bandgaps, but their values are found to decrease with the increase in x. The augmentation of the optical absorption range and the reduction in the recombination rate associated with the direct and indirect bandgaps reductions along with improved ferroelectric properties observed in La-doped BFO films are responsible for the enhanced PV characteristics. This work will provide an insight into the ferroelectric PV effect observed at the MPB composition which can be extended to other systems so as to exhibit PV properties suitable for device applications.

See supplementary material for the enlarged portion of the deconvoluted diffraction patterns near the 2θ angles 31°–33°, Raman spectra, detailed analysis of absorption peaks observed in BFO, Tauc's plots for the BLFO films of $x = 0.05$, 0.10, 0.15, 0.20, 0.25, and 0.30 compositions, domain evolution and domain switching patterns for all films, *J*–*V* plots for $x = 0.05$, 0.10, 0.15, and 0.20 compositions in poled and unpoled states, and the effect of multiple poling reversal on the PV effect of BFO films.

The authors acknowledge Dr. N. V. Giridharan and Mr. D. Dhayanithi, Department of Physics, National Institute of Technology, Tiruchirappalli 620015, India, for *P-E* loop measurements.

REFERENCES

[1]K. Ranabhat, L. Patrikeev, A. A. Revina, K. Andrianov, V. Lapshinsky, and E. Sofronova, J. Appl. Eng. Sci. **14**, 481 (2016).
[2]A. G. Chynoweth, Phys. Rev. **102**, 705 (1956).
[3]A. M. Glass, D. von der Linde, and T. J. Negran, Appl. Phys. Lett. **25**, 233 (1974).
[4]W. T. H. Koch, R. Munser, W. Ruppel, and P. Würfel, Solid State Commun. **17**, 847 (1975).
[5]J. Zhang, X. Su, M. Shen, Z. Dai, L. Zhang, X. He, W. Cheng, M. Cao, and G. Zou, Sci. Rep. **3**, 2109 (2013).
[6]J. E. Spanier, V. M. Fridkin, A. M. Rappe, A. R. Akbashev, A. Polemi, Y. Qi, Z. Gu, S. M. Young, C. J. Hawley, D. Imbrenda, G. Xiao, A. L. Bennett-Jackson, and C. L. Johnson, Nat. Photonics **10**, 611 (2016).
[7]I. Grinberg, D. V. West, M. Torres, G. Gou, D. M. Stein, L. Wu, G. Chen, E. M. Gallo, A. R. Akbashev, P. K. Davies, J. E. Spanier, and A. M. Rappe, Nature **503**, 509 (2013).
[8]H. T. Yi, T. Choi, S. G. Choi, Y. S. Oh, and S.-W. Cheong, Adv. Mater. **23**, 3403 (2011).
[9]X. Yang, X. Su, M. Shen, F. Zheng, Y. Xin, L. Zhang, M. Hua, Y. Chen, and V. G. Harris, Adv. Mater. **24**, 1202 (2012).
[10]S. Pal, A. B. Swain, P. P. Biswas, D. Murali, A. Pal, B. R. K. Nanda, and P. Murugavel, Sci. Rep. **8**, 8005 (2018).
[11]A. Zenkevich, Y. Matveyev, K. Maksimova, R. Gaynutdinov, A. Tolstikhina, and V. Fridkin, Phys. Rev. B **90**, 161409 (2014).
[12]S. M. Young and A. M. Rappe, Phys. Rev. Lett. **109**, 116601 (2012).
[13]M. Nakamura, S. Horiuchi, F. Kagawa, N. Ogawal, T. Kurumaji, Y. Tokura1, and M. Kawasaki, Nat. Commun. **8**, 281 (2017).
[14]V. I. Belinicher and B. I. Sturman, Ferroelectrics **83**, 29 (1988).
[15]W. Ji, K. Yao, and Y. C. Liang, Adv. Mater. **22**, 1763 (2010).
[16]A. B. Swain, M. Rath, S. Pal, M. S. R. Rao, V. Subramanian, and P. Murugavel, Appl. Phys. Lett. **113**, 233902 (2018).
[17]P. P. Biswas, Ch. Thirmal, D. Duraisamy, G. N. Venkatesan, S. Venkatachalam, and P. Murugavel, Appl. Phys. Lett. **110**, 192906 (2017).
[18]M. Qin, K. Yao, and Y. C. Liang, Appl. Phys. Lett. **93**, 122904 (2008).
[19]T. Qi, I. Grinberg, and A. M. Rappe, Phys. Rev. B **83**, 224108 (2011).
[20]L. Jiang, I. Grinberg, F. Wang, S. M. Young, P. K. Davies, and A. M. Rappe, Phys. Rev. B **90**, 075153 (2014).
[21]H. Matsuo, Y. Noguchi, and M. Miyayama, Nat. Commun. **8**, 207 (2017).
[22]J. Wang, J. B. Neaton, H. Zheng, V. Nagarajan, S. B. Ogale, B. Liu, D. Viehland, V. Vaithyanathan, D. G. Schlom, U. V. Waghmare, N. A. Spaldin, K. M. Rabe, M. Wuttig, and R. Ramesh, Science **299**, 1719 (2003).
[23]V. Železný, D. Chvostová, L. Pajasová, I. Vrejoiu, and M. Alexe, Appl. Phys. A **100**, 1217 (2010).
[24]S. Y. Yang, L. W. Martin, S. J. Byrnes, T. E. Conry, S. R. Basu, D. Paran, L. Reichertz, J. Ihlefeld, C. Adamo, A. Melville, Y.-H. Chu, C.-H. Yang, J. L. Musfeldt, D. G. Schlom, J. W. Ager III, and R. Ramesh, Appl. Phys. Lett. **95**, 062909 (2009).
[25]T.-L. Yan, B. Chen, G. Liu, R.-P. Niu, J. Shang, S. Gao, W.-H. Xue, J. Jin, J.-R. Yang, and R.-W. Li, Chin. Phys. B **26**, 067702 (2017).
[26]Y. Ukai, S. Yamazaki, T. Kawae, and A. Morimoto, Jpn. J. Appl. Phys. Part 1 **51**, 09LE10 (2012).
[27]V. S. Puli, D. K. Pradhan, R. K. Katiyar, I. Coondoo, N. Panwar, P. Misra, D. B. Chrisey, J. F. Scott, and R. S. Katiyar, J. Phys. D: Appl. Phys. **47**, 075502 (2014).
[28]S.-T. Zhang, Y. Zhang, M.-H. Lu, C.-L. Du, Y.-F. Chen, Z.-G. Liu, Y.-Y. Zhu, and N.-B. Ming, Appl. Phys. Lett. **88**, 162901 (2006).
[29]D. Lee, M. G. Kim, S. Ryu, H. M. Jang, and S. G. Lee, Appl. Phys. Lett. **86**, 222903 (2005).
[30]C.-J. Cheng, D. Kan, V. Anbusathaiah, I. Takeuchi, and V. Nagarajan, Appl. Phys. Lett. **97**, 212905 (2010).
[31]D. Kan, C.-J. Cheng, V. Nagarajan, and I. Takeuchi, J. Appl. Phys. **110**, 014106 (2011).
[32]I. O. Troyanchuk, D. V. Karpinsky, M. V. Bushinsky, V. A. Khomchenko, G. N. Kakazei, J. P. Araujo, M. Tovar, V. Sikolenko, V. Efimov, and A. L. Kholkin, Phys. Rev. B **83**, 054109 (2011).
[33]S. B. Emery, C.-J. Cheng, D. Kan, F. J. Rueckert, S. P. Alpay, V. Nagarajan, I. Takeuchi, and B. O. Wells, Appl. Phys. Lett. **97**, 152902 (2010).
[34]L. You, F. Zheng, L. Fang, Y. Zhou, L. Z. Tan, Z. Zhang, G. Ma, D. Schmidt, A. Rusydi, L. Wang, L. Chang, A. M. Rappe, and J. Wang, Sci. Adv. **4**, eaat3438 (2018).
[35]R. V. Pisarev, A. S. Moskvin, A. M. Kalashnikova, and T. Rasing, Phys. Rev. B **79**, 235128 (2009).
[36]S. R. Basu, L. W. Martin, Y. H. Chu, M. Gajek, R. Ramesh, R. C. Rai, X. Xu, and J. L. Musfeldt, Appl. Phys. Lett. **92**, 091905 (2008).
[37]J. F. Ihlefeld, N. J. Podraza, Z. K. Liu, R. C. Rai, X. Xu, T. Heeg, Y. B. Chen, J. Li, R. W. Collins, J. L. Musfeldt, X. Q. Pan, J. Schubert, R. Ramesh, and D. G. Schlom, Appl. Phys. Lett. **92**, 142908 (2008).
[38]J. B. Neaton, C. Ederer, U. V. Waghmare, N. A. Spaldin, and K. M. Rabe, Phys. Rev. B **71**, 014113 (2005).
[39]P. Baettig, C. Ederer, and N. A. Spaldin, Phys. Rev. B **72**, 214105 (2005).
[40]S. J. Clark and J. Robertson, Appl. Phys. Lett. **90**, 132903 (2007).
[41]J. I. Pankove, *Optical Processes in Semiconductors* (Dover Publications, 1971), p. 422.
[42]G. Catalan and J. F. Scott, Adv. Mater. **21**, 2463 (2009).
[43]M. D. Scafetta, A. M. Cordi, J. M. Rondinelli, and S. J. May, J. Phys.: Condens. Matter **26**, 505502 (2014).
[44]K. Carl and K. H. Hardtl, Phys. Status Solidi A **8**, 87 (1971).